

Estimation of Influence of Target Obliquity on Efficiency of PELE Ammunition

Alan Catovic¹, Faruk Razic¹

¹ University of Sarajevo - Mechanical Engineering Faculty, Vils. set. 9, Sarajevo, Bosnia and Herzegovina

Abstract – In the available literature, no research on target obliquity influence on terminal ballistics of PELE could be found. This study aimed to give an insight into this phenomenon. As a part of the research, numerical simulations were performed with four different target obliquity angles, namely 0°, 30°, 45°, and 60°. Before the simulations, the numerical model was validated with available experimental data. It was shown that the case of a target inclination of 30° is the most effective in stopping PELE ammunition, for the given type of materials and design, because it shows the lowest number of fragments created and also the lowest velocity of fragments, with large number of fragments lost in front of the target. Target obliquity leads to the asymmetric deformation of the projectile and at larger target obliquities a good part of the jacket and core is fragmented and lost in front of the target. Residual velocity of projectile is smaller for larger target obliquities. The deformation of the aluminum core is significant for larger target obliquities. Perforation time for larger target obliquity angles is longer. The lower side of the projectile casing is more deformed than the upper side for target obliquities larger than 0°. Fragments that originate from the front part of the projectile jacket are faster compared to fragments originating from the projectile lower sections. The perforation hole is significantly larger for higher target obliquity angles than for smaller ones. For a 60° inclination of the target, several massive fragments are created in front of the target.

Keywords – PELE, armor penetration, simulation.

1. Introduction

By utilizing the differences in material properties between the projectile casing and the inner core, the PELE (Penetration with Enhanced Lateral Efficiency) projectile is a relatively new concept (first test was done in 1996) and also safe (high explosives are not used) type of armor piercing projectile that can convert part of the translational kinetic energy into radial kinetic energy.

Aluminum and plastic (i.e. polyethylene) are common examples of materials with a relatively low density used for the inner core (filler), whereas heavier metals like steel and tungsten alloy are typically used for the casing of projectiles [1], [2]. The fragmentation effect and penetrating ability are the two primary damaging features of the PELE projectile (Fig. 1).



Figure 1. PELE projectile 25x137 mm (casing in lower part filled with spherical fragments) [5]

There are four stages to the PELE penetrator's behavior. The core material is enclosed in the first stage as a result of the casing and core having differing kinetic energies. This causes the core's pressure to increase, which causes the casing around it to expand in the second step. In the third phase the high-density casing disintegrates (lower fragmentation is observed when using the core with higher density). A fourth step is an interaction between the core and the target plug (a low-density core can be significantly eroded by the target plug during the process) [1].

DOI: 10.18421/TEM134-11

<https://doi.org/10.18421/TEM134-11>


Corresponding author: Alan Catovic,
University of Sarajevo - Mechanical Engineering Faculty,
Wilsonovo setaliste 9, Sarajevo, Bosnia and Herzegovina
Email: catovic@mef.unsa.ba

Received: 01 April 2024.

Revised: 12 August 2024.

Accepted: 02 September 2024.

Published: 27 November 2024.

 © 2024 Alan Catovic & Faruk Razic; published by UIKTEN. This work is licensed under the Creative Commons Attribution-NonCommercial-NoDeriv 4.0 License.

The article is published with Open Access at <https://www.temjournal.com/>

It is the only known projectile type that employs hydrodynamic pressure, a technique that eliminates the need for explosives, to transform the axial velocity of the projectile into radial velocity (of fragments). It should be noted that projectile lateral efficiency lowers its overall penetration performance [1].

Examples of PELE medium caliber ammunition, currently in production, include Rheinmetall 20x102 mm, 25x137 mm (Fig. 1), 27x145 mm, 30x173 mm [3].

Rheinmetall company also produces large caliber 120 mm PELE (inert) tank ammunition (Fig. 2); The low-density core within the projectile compresses so much when it strikes its target that the projectile casing bursts, creating many fragments. When it comes to semi-hard targets, this is quite helpful. PELE can be retrofitted to armor-piercing or multipurpose ammunition [6]. Terminal effects of 120 mm PELE ammunition on different targets (double reinforced concrete with container, RHA NATO target at 60°, clay brick wall, Armored Observation Vehicle) can be seen in [7]. This ammunition offers a possibility of precise and effective engagement of several targets with a minimum of collateral damage.

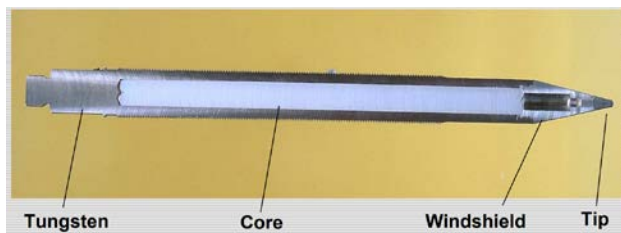


Figure 2. Sectional view of the PELE Penetrator of 120 mm DM 33 KE ammunition [7]

The PELE concept is expanded upon by the active lateral penetrator. With an active lateral penetrator, a tiny quantity of explosive that can be detonated regardless of the location of the charge is used to achieve increased ballistic efficiency during the impact on the target.

Factors influencing PELE penetration process are: projectile and target materials (density, sound velocity), impact velocity, projectile design, target thickness, target obliquity, projectile yaw angle.

There is no publicly available study on target obliquity's impact on PELE's terminal ballistics. Therefore, the purpose of this study is to shed some light on this subject.

The study is divided into several sections: a review of the literature, a validation of the numerical model with available experimental data, and a section with research and analysis of target obliquity influence on terminal ballistics parameters of PELE.

2. The Review of Literature

Paulus and Schirm [1] carried out several test (different types and thicknesses of targets, and different projectile components materials) with PELE projectiles in the velocity range between 900 and 3000 m/s (targets had no obliquity). They determined (a system of coordinates is established to interpret the radiographs) the residual velocity of the projectile and radial velocity of fragments, as main parameters of PELE projectiles. A brief summary of material data is also provided.

Ding *et al.* [2] tried to realistically estimate the penetration process of PELE (Penetration with Enhanced Lateral Efficiency) projectile, using stochastic failure and crack-softening algorithms in numerical simulations (Ansys Autodyn). Material parameters of these models were calibrated and successfully used (good agreement with experimental data).

In comparison to traditional PELE projectiles, Zhou *et al.* [8] found in their research that using polytetrafluoroethylene (PTFE)/Al as a reactive material (together with a truncated conical head) increased residual projectile velocity by up to 21% and fragment damage range by up to 43%.

Xu *et al.* [9] used simulations and tests to examine the important PELE projectile parameters (casing wall thickness, casing and core material, and casing angle) on the target (reinforced concrete) hole diameter. Nylon 1010 and 50SiMnVB were the materials used for the core and case.

The impact of casing fracture strain on the fragmentation effect of PELE projectile was experimentally investigated by Liu *et al.* [10]. They demonstrated that while the fragmentation effect is increased as projectile impact velocity increases, the critical fracture strain of the projectile casing decreases as impact velocity increases.

To describe the penetrating capability of the PELE projectile, Ding *et al.* [11] created four distinct inner core material combinations. The projectile's residual length and velocity, as well as the fragments' radial velocity and scattering radius, were next examined using simulations. It is discovered i.e. that appropriately raising the strength of the front inner core material may increase the radial velocity and radial scattering radius of fragments.

Cheng *et al.* [12] performed tests of steel and aluminum alloy target plates by PELE in order to study the failure characteristics of metal target plate.

In addition to observing the macroscopic morphology of the perforation on the target plate and the plug, the perforation wall was polished and sliced in order to use metallographic and scanning electron microscopy (SEM) to determine the distribution and progress of the fractures in the wall.

PELE's ductile perforation of the metal target plate differs from that of conical-nosed projectiles' and flat-nosed projectiles' punching failures.

Fan *et al.*'s research [13] showed that, for a given impact velocity of PELE, the target plate's thickness and shock impedance both enhance the radial velocities of the dispersed fragments. Their research revealed a correlation between the max radial velocity of fragments and the casings's and core's bulk modulus, and Poisson's ratio, with the max radial velocity increasing as both rise.

Jo and Lee [14] created numerical models of the projectile and the target in order to investigate the properties of PELE projectiles. They simulated the process of employing PELE to penetrate an aluminum alloy 2024 target. For various core materials, the scattering properties following PELE penetration of the aluminum alloy target were examined. Using the stochastic failure criteria, the explicit finite element analysis of PELE fragmentation was accomplished in AUTODYN-3D.

Ding *et al.* [15] used the shock wave theory to investigate the mechanism of a PELE projectile piercing a thin metal target plate. They also established a theoretical model of axial residual velocity. The kinetic energy increase of the target plug in the impact zone, the internal energy increase of the outer casing and inner core, and the energy dissipation of the projectile against the target plate comprised the three components of the energy loss during the penetration phase.

Wu *et al.* [16] simulated 60 mm diameter PELE penetrating the target. They showed that with the increase of the core radius in PELE projectile, the radial velocity of the fragments also increases.

In order to increase the fragmentation impact of PELE projectiles, Ding *et al.* [17] investigated the application of reactive materials to the inner core of PELE projectiles. Additionally, a theoretical model of the reactive core PELE projectile fragments' radial scattering velocity was given.

A theoretical model was developed by Ji and Wang [18] to forecast the PELE's residual velocity following target penetration. The ballistic limit velocities of PELE penetrating into steel (#45) and aluminum alloy (20124) targets are also provided by adapting the De Marre formula. They reported that different types of core materials have little influence on penetration capability of PELE.

Using six sets of scenarios, Ding *et al.* [19] evaluated and examined the destructive power of the standard PELE projectile and the truncated cone-shaped PELE projectile. The primary assessment indicators employed were the fragmentation effect and penetrating ability.

The truncated cone-shaped PELE projectile was discovered to have a better fragmentation effect than the standard PELE projectile.

Tu *et al.* [20] used 35GrMnSiA and nylon as the casing and the core of PELE, respectively, for vertical impact into armor plates (5-25mm thick), with an impact velocity of 770 ± 20 m/s. They found that when armor plate thickness increases, axial velocity decreases approximately linearly.

A unique charge structure was presented by Yin *et al.* [21] that can generate an explosively formed projectile (EFP) or a penetrator with increased lateral effect (PELE) with different initiation modes.

An analytical model of fragmentation of PELE ammunition was provided by Verreault [22]. The material state is determined by the Rankine-Hugoniot relations and the model's assumption of uniaxial strain in the core. The radial rarefaction emanating from the casing outer surface is taken into consideration, together with the shock and rarefaction wave interactions at the target free surface and the core/target interface. ANSYS Autodyn software is used in all used numerical simulations.

In [23] modelling fragmentation in Autodyn was described. The primary cause of void expansion is volumetric tensile stress: in a triaxial stress state, stress is dominant factor in failure, whereas in a uniaxial stress state, strain is dominant factor. Using the principal stress failure, a number of simulations of the high-velocity impact of metallic projectiles against thin targets were reported in [23]. The material's critical spall stress model by Grady was applied. The imposition of material heterogeneity was accompanied by micro defects that are the source of fracture. One way to achieve this numerically is to set the material's failure strain to random and give each cell in the numerical model a distinct failure strain. This was achieved by Mott distribution model, in which the constants C and are used to predict the probability of fracture. So, the fragmentation from tests was replicated by introducing variability into material's failure characteristics. Material fragmentation due to dynamic loading occurs in three sequential steps [23]:

- Local failure occurs when a material's capacity to withstand stress or strain is exceeded, resulting in local cracking in brittle materials and/or void development in ductile materials.

- The expansion of the failed areas as a result of the surrounding stress/strain field, which is impacted by the failed area itself.

- The material breaks apart into finite fragments due to the coalescence of the various areas that failed.

3. Research and Analysis

This section presents main part of the paper - numerical simulations of PELE penetrator. Here, first subsection presents model validation and following subsection deals with influence of incidence angle of PELE penetrator on its terminal ballistics parameters.

3.1. The Numerical Model Validation

The simulations are done in Ansys Autodyn, using a Lagrange processor. In this research, the numerical model was first validated with experimental results presented in [1]. For the validation study, the following material parameters were taken into account: the projectile casing was made of tungsten alloy (D-180 K in [1]), the inner core was made of aluminum alloy (A-G3 in [1]), and the target plate was made of steel (XC48 in [1]). Following is a brief explanation of materials and material models used in simulation for validation.

D180K alloy, from [1], is a tungsten-nickel-iron Alloy (95% WNiFe). It has high density, high strength, and can be precision formed and machined. Typical applications include aviation and aerospace, the optical industry, collimator and shielding components for X-ray and gamma radiation protection, balancing weights in motors and drive components, vibration dampers in motors and drive components, etc. As a material similar to D180 K, tungsten alloy with 4% nickel and 2% iron (94% WNiFe or W-4Ni-2Fe) is chosen for numerical simulations since it is similar (in alloying element percents) and its main constitutive material parameters (equation of state and Steinberg-Guinan constitutive model) are already present in Autodyn material library (Tables 1 and 2). Theoretical details on the shock equation of state and Steinberg-Guinan strength model can be found in [24]. Spall strength (needed for failure modeling) for WNiFe alloy in this study was determined using brittle spall model by Grady [2], [25], since WNiFe alloys under dynamic loading show characteristics of brittle fracture [34]. Brittle spall strength, according to Grady's model, can be determined using following expression [25]:

$$P_s = (3\rho c_0 K_c^2 \dot{\epsilon})^{1/3} \quad (1)$$

Here ρ is material density (18000 kg/m³ for this alloy), c_0 is bulk sound velocity (4030 m/s for tungsten heavy alloy; Table 1), K_c is fracture toughness (value of 90 MPa·m^{1/2} is adopted for tungsten heavy alloy, as reported in [4], and $\dot{\epsilon}$ is strain rate (chosen as 10⁴ s⁻¹, similar to [2]). Using this data, spall strength for WNiFe alloy, obtained with expression (1), is 2.6 GPa.

This spall strength value corresponds well with values reported in [26]. Obtained spall strength value for heavy tungsten alloy is used in principal tensile stress failure model in Autodyn, together with stochastic failure model, similar to simulations reported in [2], [23]. Namely, to simulate fragmentation of material, a degree of material heterogeneity must be imposed. Microscopic imperfections in real materials are a natural source of failures and the beginning of cracking. Randomizing the material's failure stress is one way to replicate this numerically. This attribute is used to determine the variation in failure stress using a Mott distribution [27]:

$$P(\epsilon) = 1 - e^{\left[-\frac{C}{\gamma}(e^{\gamma\epsilon}-1)\right]} \quad (2)$$

Here P is the probability of fracture, ϵ is the strain, and C and γ are material constants. Many of the failure models can be combined with the stochastic failure option. Both the distribution seed type and the magnitude of the stochastic variance, γ , must be specified. Constant γ for tungsten heavy alloy, used in this study, was 36.5, as reported in [2]. Generally, every time a simulation runs, a different distribution will be determined if "random" option is used but every solution will utilize the same distribution if the "fixed" option is used [27] (in this paper, option "fixed" was also used).

Aluminum A-G3 (or aluminum 5754), used as a core material in [1], has magnesium as the main alloying element (up to 3.6%). This alloy can have yield strength, depending on temper, from 80 to 230 MPa, and tensile strength from 190 to 330 MPa [28]. In the simulations, aluminum alloy 5083-H116 (Mg content up to 4.9% by weight) was used since it also has magnesium as the main alloying element. Generally, aluminum alloy 5083-H116 is high-strength alloy, commonly employed in marine applications, protective structures, gas/oil pipes, drilling rigs, towers, pressure vessels, transportation, ordnance, and armor plate [29]. Equation of state (Table 1), Johnson-Cook strength model (Table 3), and Johnson-Cook failure model (Table 4) data are available for this alloy in [30]. Theory on Johnson-Cook strength and Johnson-Cook failure models can be found in [31].

Steel XC48, used as the target material in [1], is regarded as steel C45 or AISI 1045/1049. This is structural, medium carbon steel (0.42-0.5% C) that can be used as-treated (quenched and tempered) or as-annealed (normalized), depending on the level of desired mechanical characteristics. It is also suitable for surface hardening. This is a medium-strength steel with good machinability and tensile properties. Tensile strength is usually 570-700 MPa [23], with 720 MPa reported in [1]. In the simulations, steel 4340 is used as an approximation for this steel.

Equation of state (Table 1), Johnson-Cook strength model (Table 3), and Johnson-Cook failure model data (Table 4) are available for this steel in Autodyn library, and in [32], [33].

In summary, the equation of state (EoS) for all materials considered was shock EoS (Mie-Grüneisen), with parameters presented in Table 1. Constitutive model parameters for mentioned materials are presented in Tables 2 and 3. Johnson-Cook failure model constants for projectile core and target materials are presented in Table 4. Maximal principal stress in failure model for tungsten alloy (projectile casing) is 2.6 GPa, and this model was used together with stochastic failure model ($\gamma=36.5$).

Dimensions of projectile parts and targets were taken from [1]. Projectile core diameter was 6 mm, and casing diameter was 10 mm (2 mm casing thickness).

Projectile length was 50 mm, and the target thickness 3 mm. The 3D numerical simulations were used with 1/2 of the full domain (one symmetry plane) for reduced calculation time (Fig. 1).

As a part of the validation process, simulations were performed with mesh size where hexagonal elements were 0.3 mm in size (Fig. 1), with total of 556595 elements in the mesh. The initial condition was a projectile impact velocity (925 m/s), the same as reported in experimental research [1]. The boundary condition was fixing the target on its outer edge (parallel to the projectile symmetry axis).

Erosion of elements was controlled by material failure and instantaneous geometric strain (value of 1.5) for all materials. The inertia of eroded elements was retained throughout the simulation. The time of simulation was 100 ms since during this time projectile perforates the target.

Table 1. Gruneisen shock EOS data for materials

Material	Density (g/cm ³)	Gruneisen coefficient	c ₀ (m/s)	s
W4Ni2Fe [Autodyn library]	18.0	1.67	4030	1.24
Steel/iron [Autodyn library]	7.82	1.93	4570	1.49
Al. alloy 5083-H116 [24]	2.65	1.97	5340	1.40

Table 2. Steinberg-Guinan model for tungsten heavy alloy

Material	Shear modulus (kPa)	Yield stress (kPa)	Maximum yield stress (kPa)	Hardening constant; Hardening exponent	Derivative dG/dP	Derivative dG/dT (kPa/K)	Derivative dY/dP	Melting temp. (K)
W4Ni2Fe	1.45·10 ⁸	1.87·10 ⁶	4·10 ⁶	7.7; 0.13	1.494	-2.204·10 ⁴	0.01926	2.263·10 ³

Table 3. The constitutive Johnson-Cook model for projectile core and target

Material	A (MPa)	B (MPa)	n	C	m
Steel 4340 [Autodyn library]	792	510	0.26	0.014	1.03
Aluminum alloy 5083-H116 [24]	167	596	0.551	0.001	0.859

Table 4. Constants for the Johnson-Cook failure model for projectile core and target

Material	D ₁	D ₂	D ₃	D ₄	D ₅
Steel 4340 [Autodyn library]	0.05	3.44	-2.12	0.002	0.61
Aluminum alloy 5083-H116 [24]	0.0261	0.263	-0.349	0.147	16.8

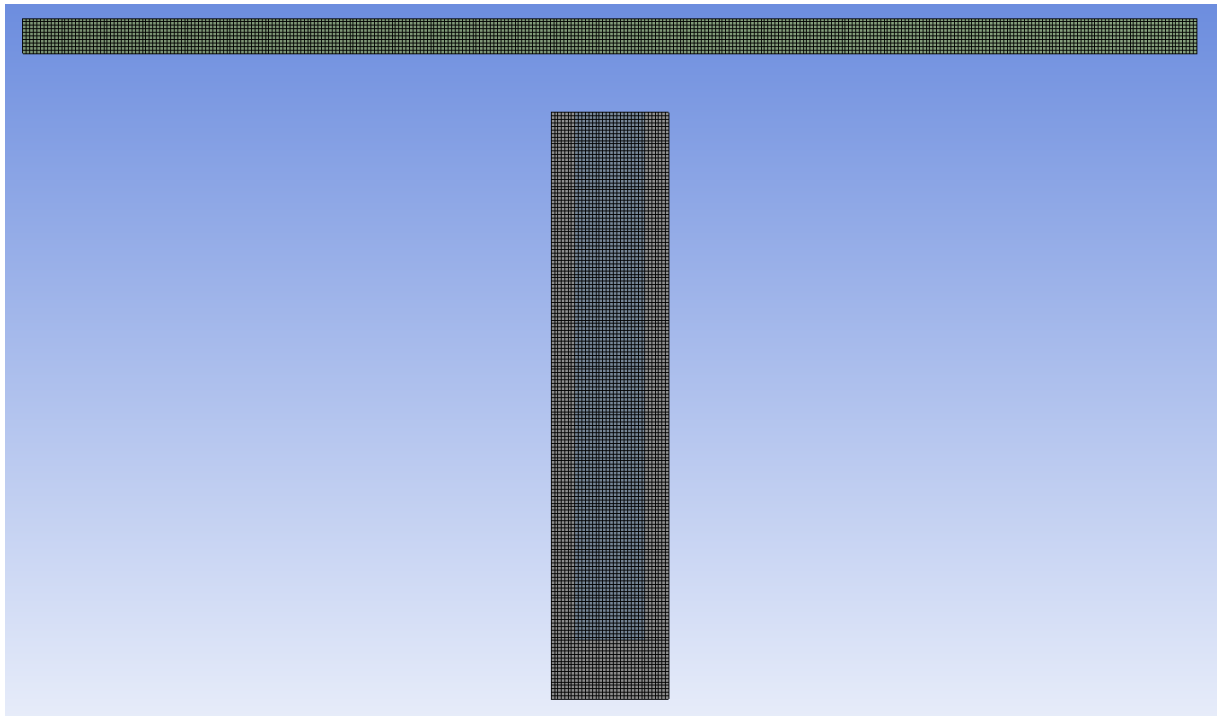


Figure 3. Numerical mesh used in simulations (element size 0.3 mm, $\frac{1}{2}$ of the full 3D domain)

The result of the simulation (impact velocity 925 m/s) for the steel target, tungsten heavy alloy casing, and aluminum alloy core (parameters presented in Tables 1-4) can be seen in Figs. 2 and 3. Fig. 2 presents the residual velocity contours for PELE after the perforation while Fig. 3 shows the fragment velocity curve, where the fragment corresponding to the mesh element in the middle of the casing was taken into account. In the lower part of Fig. 3, the PELE section was shown to easily identify the parts of the casing for which the fragment velocity was considered (segments up to half of casing length).

In experimental research [1], it was obtained for the same projectile and target that the residual velocity (after exiting the target) was 895 m/s (as measured in the test). In this study (Fig. 2), the residual velocity of the projectile was in the range of 886.2 m/s (lower part of PELE) to 891.8 m/s (frontal part of PELE), which equates to max. relative error of 0.9% compared to results from the work presented in [1].

The maximum velocity of fragments (perpendicular to the axis of the projectile) obtained in the simulation was 183.8 m/s (Fig. 3), while in the test [1] it was measured as 184 m/s, which gives max relative error of 0.1%.

Also, the fragmentation process and „opening“ of the casing of PELE after the penetration are quantitatively in good agreement to the ones recorded (X-ray images) in the experimental test [1].

In [15], post-failure images of the PELE projectile are shown where it can be seen that the aluminum core is deformed after the perforation of the target plate but it is not fractured. Also, in [1], when reviewing post-failure X-ray images one can see that the aluminum core is not significantly eroded or deformed after the perforation for this impact velocity. This was also observed in this study - the aluminum core was not much deformed or eroded after the perforation of target (Fig. 2).

This all means that the numerical (simulation) model, used further on in this research, was successfully validated with available experimental data.

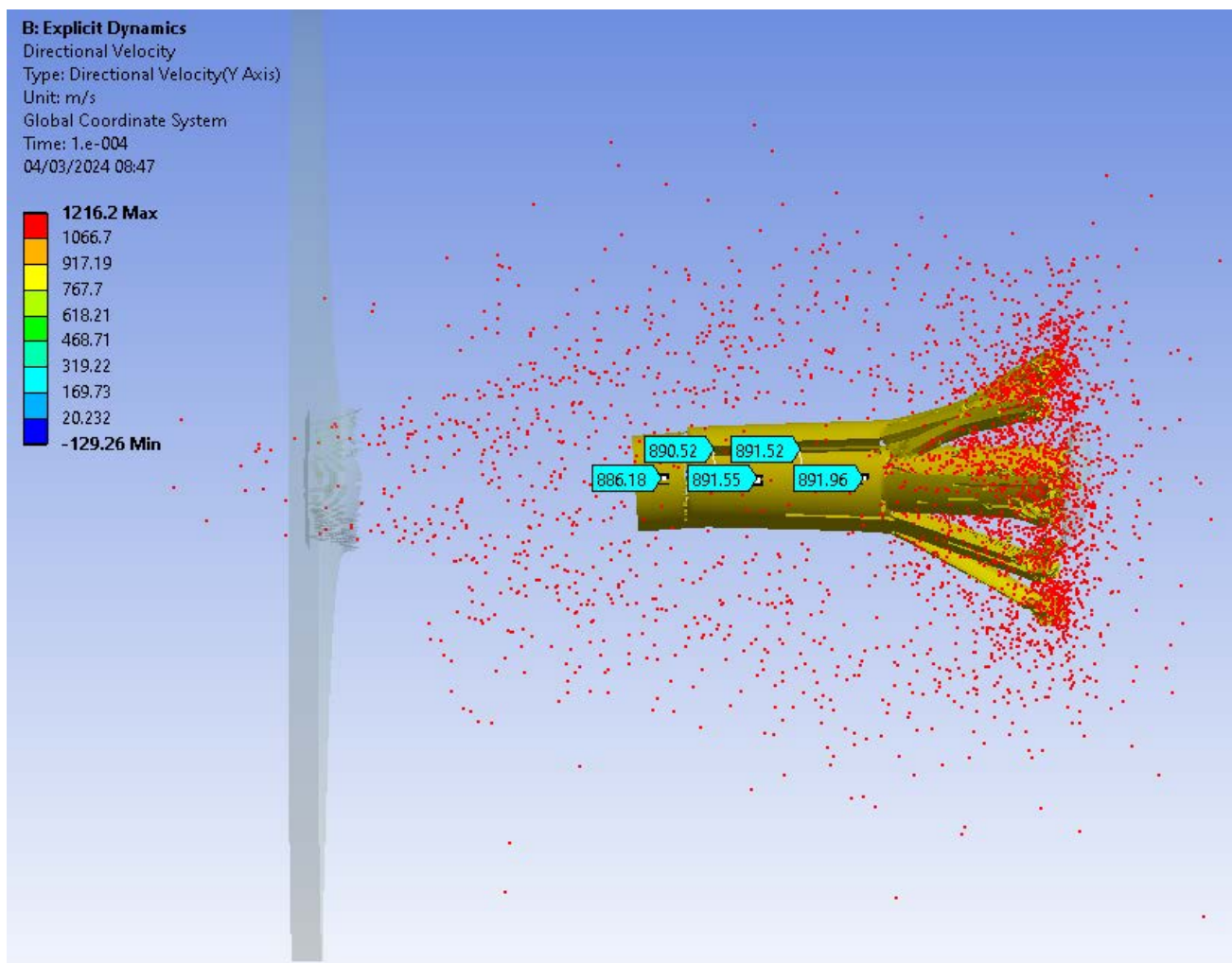


Figure 4. Result of validation simulation - velocity contours of PELE ammunition (penetrator) after perforation through metal target

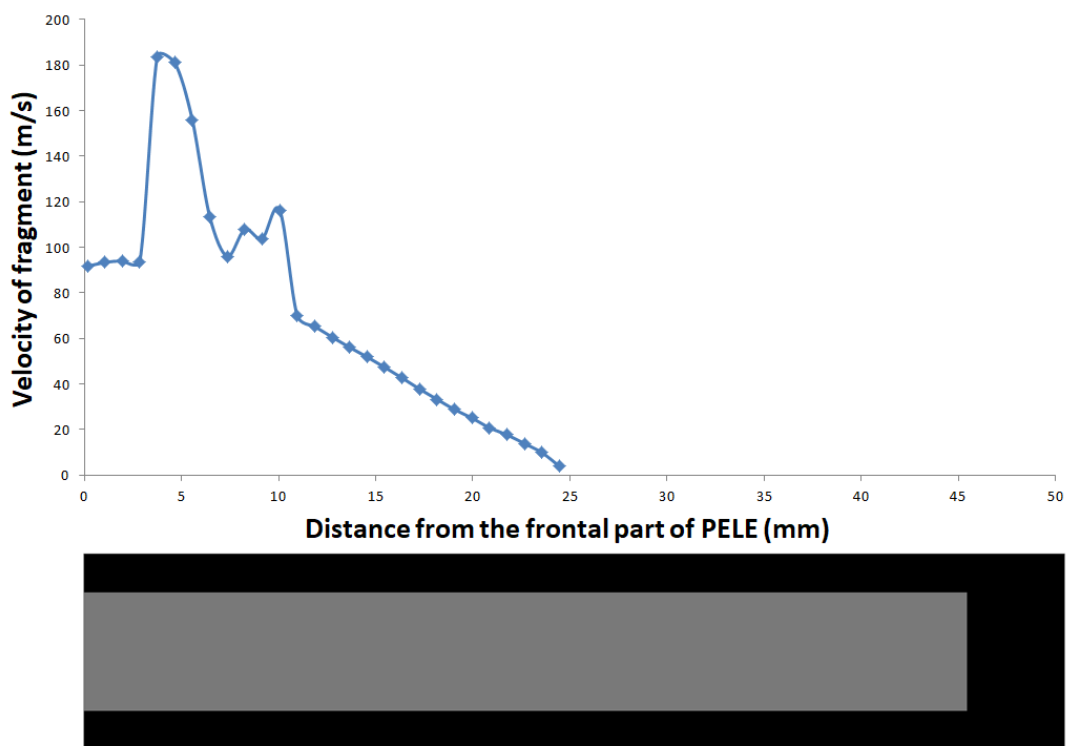


Figure 5. Result of validation simulation (fragment velocities after PELE ammunition perforation of target; image of PELE section (below) is scaled appropriately)

3.2. Research of Target Obliquity Influence on Terminal Ballistics of PELE

In the available literature, no research on target obliquity influence on terminal ballistics of PELE could be found. This study aims to give an insight into this. Numerical simulations were performed with four different target obliquity angles, namely 0° , 30° , 45° and 60° (Fig. 4). Numerical model and material parameters were the same as in the model validated in Section 3.1, only difference being the target obliquity. The initial condition was a projectile impact velocity (925 m/s).

Fig. 5 shows the processes of target penetration and casing fragmentation of PELE into the target with 0° obliquity, for four different penetration times (40 μs , 60 μs , 80 μs , and 100 μs).

From Fig. 5 it is observed that already within a few microseconds after impact, the casing starts to expand radially and cracks start to propagate. Fragments are created as the cracks merge. After 40 μs , the PELE is already half a length deep into the target, with frontal part of the casing expanding, and with fragments forming from target, core (lower number) and casing. Color of fragments in Fig. 5 indicate the fragment material type. After perforating the target, a plug (from target material) is formed. When 60 μs passes, the projectile is close to perforation, with symmetrical casing expansion, and more fragments formed. After 80 μs , a partly asymmetric fragmentation is visible, where lower right part of the PELE casing is starting to detach from the bottom of projectile (this can be because of the implementation of the Mott stochastic probability model in simulation). After 100 μs , the expansion of the casing is similar to X-ray images, presented in [1], for a given impact velocity. More fragments are created and the plug ejected from the target is visible in front of an aluminum core which was not significantly deformed. Residual velocity of projectile is in the range of 886.2 m/s (lower part of PELE) to 891.8 m/s (frontal part of PELE).

Fig. 6. shows the processes of target penetration and casing fragmentation of PELE into the target with 30° obliquity, also for different penetration times (40 μs , 60 μs , 80 μs , and 100 μs).

From Fig. 6, after 40 μs an interesting spray of fragments from the core went up, in front of the target, after the impact. An asymmetric fragment spray from the target and the jacket is also noticeable, but they are thrown with smaller velocity because they are more massive. The target plug is no longer in the central part but is located on its front lower side. After 60 μs , a considerable fragment spray is noticeable around the projectile, and its dispersion is smaller than in the case of a target angle of 0° . The deformation of the front part of the casing is also smaller. A good part of the fragments remains trapped in front of the target. After 80 μs the projectile came out in front of the target, but if it is compared with the case where the target tilt is 0° (Fig. 5), it can be seen that at this moment the projectile is closer to the target (for a target tilt angle of 30°), which means that the penetration time for this case is slightly longer (which is logical since the line of sight path is longer for the case of a target inclination of 30°). Even at this moment, the expansion of the front part of the casing is significantly smaller than in the case of a target angle of 0° . Also, a greater erosion of the aluminum core is noticeable than in the case of a target angle of 0° . The target plug was pulled even further from the front and lower side of the projectile. This (lower) side of the projectile casing is more deformed than the upper side. After 100 μs , the dispersion of fragments into space is slightly higher than after 60 μs , but it is still smaller than in the case of a target inclination of 0° (here the fragments move more radially). It is interesting that, in this case (target angle of 30°), lower part of projectile casing was not detached from the bottom of projectile even after 100 μs . Generally, for a target angle of 30° , residual velocity of projectile is in the range of 872.8 m/s (lower part of PELE) to 874.5 m/s (frontal part of PELE).

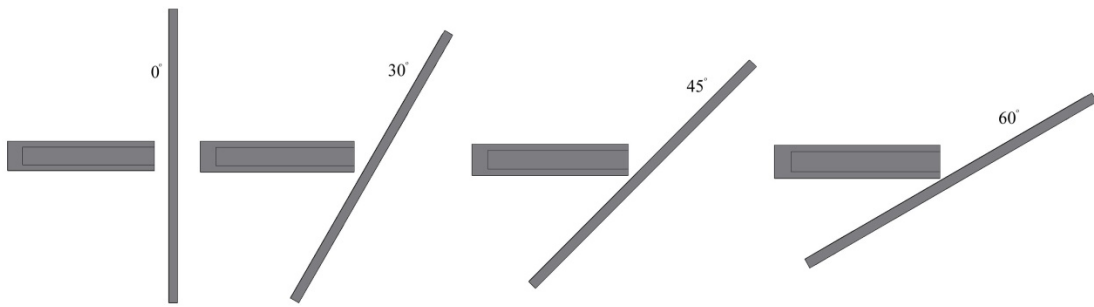


Figure 6. Four different target obliquity angles in simulations

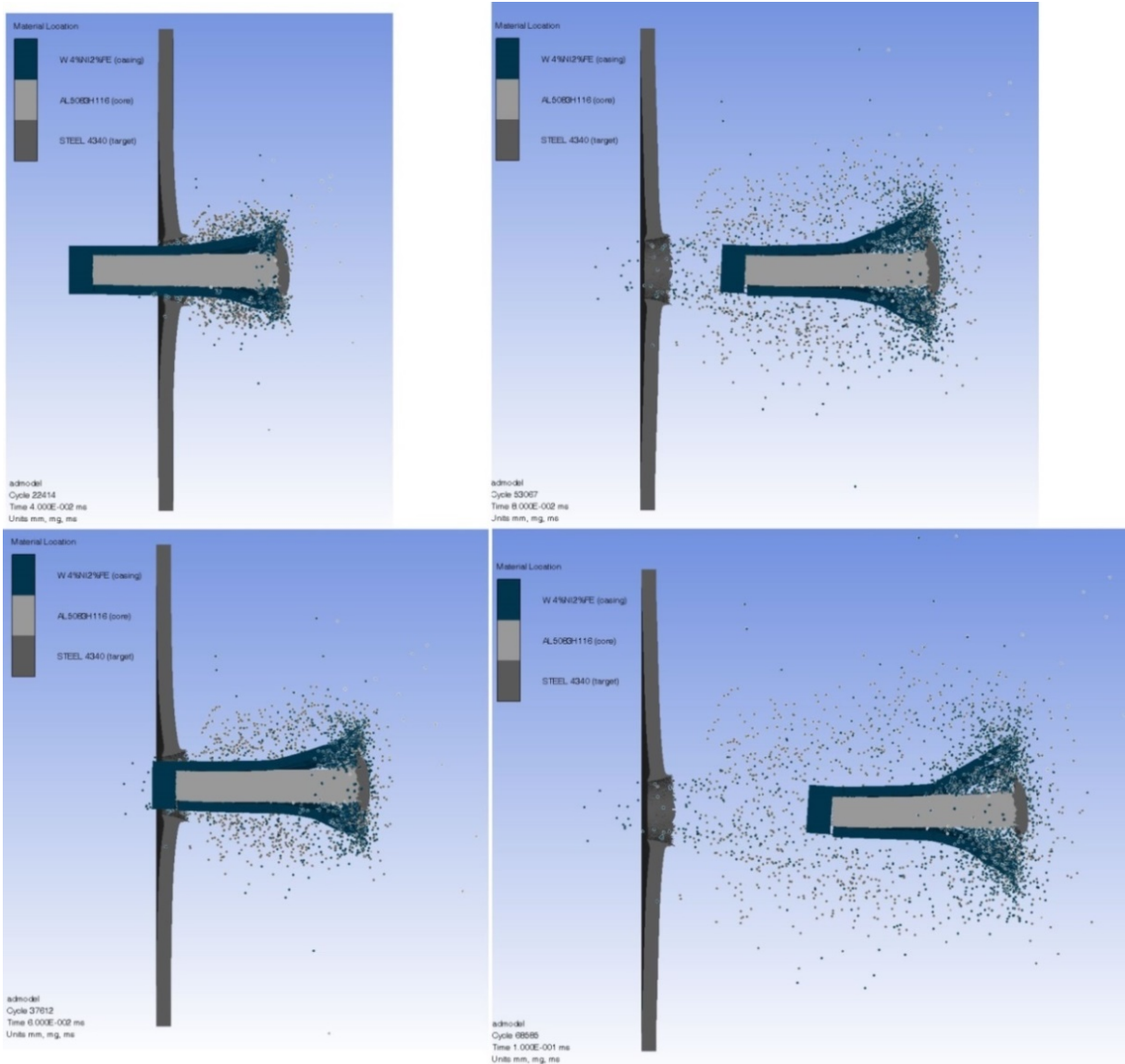


Figure 7. The processes of target penetration and casing fragmentation of PELE into the target with 0° obliquity, for four different penetration times (40 μ s, 60 μ s, 80 μ s, and 100 μ s)

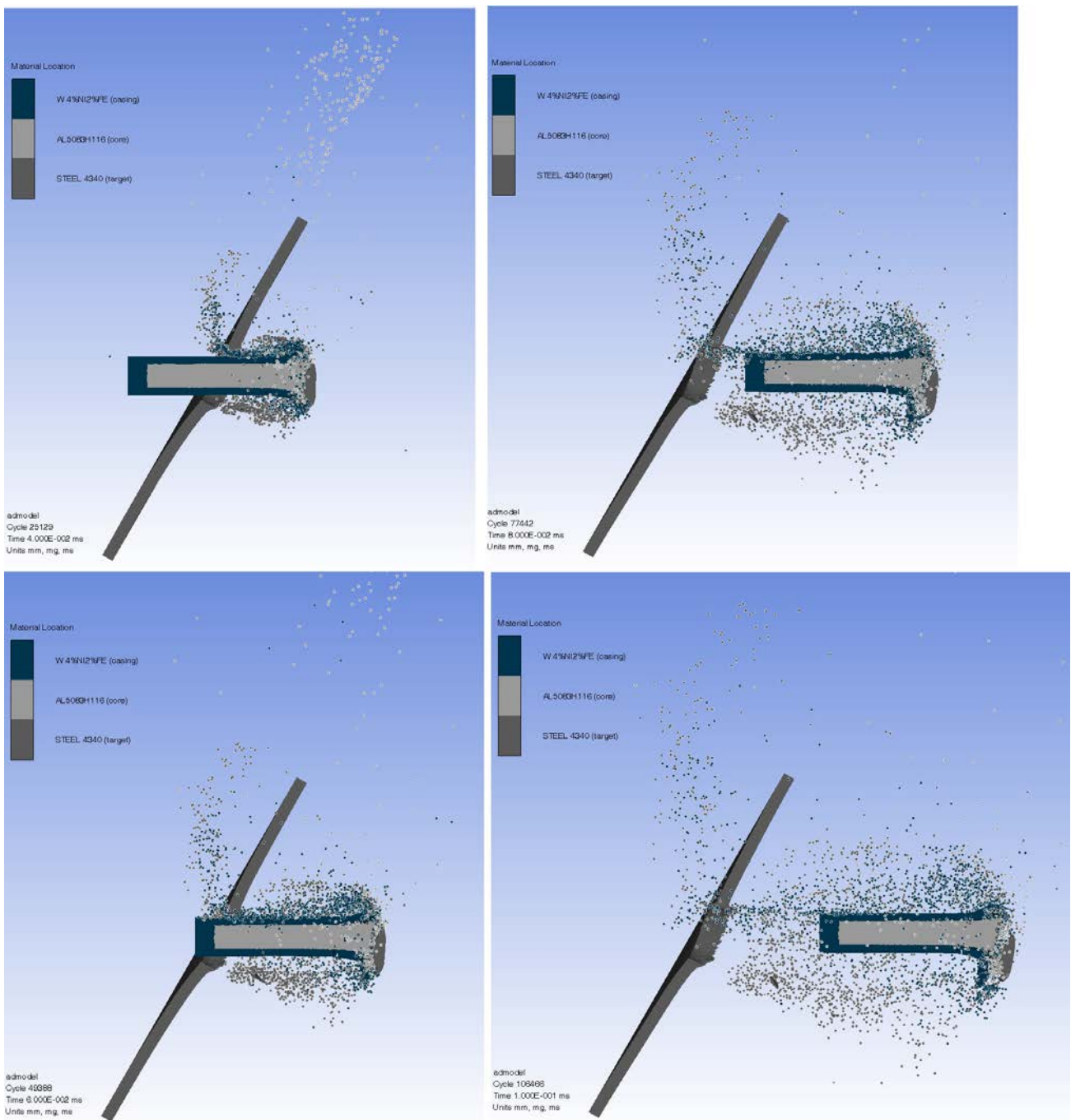


Figure 8. The processes of target penetration and casing fragmentation of PELE into the target with 30° obliquity, for different times (40μs, 60μs, 80μs, and 100 μs)

Fig. 7 shows the processes of target penetration and casing fragmentation of PELE into the target with 45° obliquity, also for different penetration times (40 μs, 60 μs, 80 μs, and 100 μs).

From Fig. 7, after 40 μs slightly less than half of the projectile has passed through the target (slower penetration than in the case of target tilts of 0° and 30°). In this case too, as with the 30° target, a significant spray of fragments from the core, target and jacket is created in front of the target upon impact.

In addition, there is greater number of fragments from the target due to the greater inclination of the target and the greater contact surface of the target and projectile. There is also greater erosion of the projectile core, and the target plug is located on the lower front side of the projectile and has an asymmetrical shape. After 60 μs, the projectile is still penetrating (different from the case when the target is inclined by 0° where the projectile is practically exiting from the target at this moment). An even greater number of fragments are created around the projectile than in the case when the target has a smaller slope but with smaller radial dispersion.

The deformation of the lower part of the casing is greater than on the upper side. Deformation is also higher than when the slope of the target is 30°. After 80 μ s, the deformation of the front part of the casing increases even more, but again it is not nearly as much as in the case when the target obliquity is 0°. The radial dispersion of the fragments is higher than at the moment of 60 μ s, but it is lower than at the target with a slope of 0°. This also applies at a time

of 100 μ s, where, also, the casing deforms even more on the frontal part. There is also a greater number of fragments from the core compared to the smaller tilting angles of the target. Also, the opening in the target (perforation hole) is much larger than for smaller target slopes. For a target angle of 45°, residual velocity of projectile is in the range of 860.6 m/s (lower part of PELE) to 864.4 m/s (frontal part of PELE).

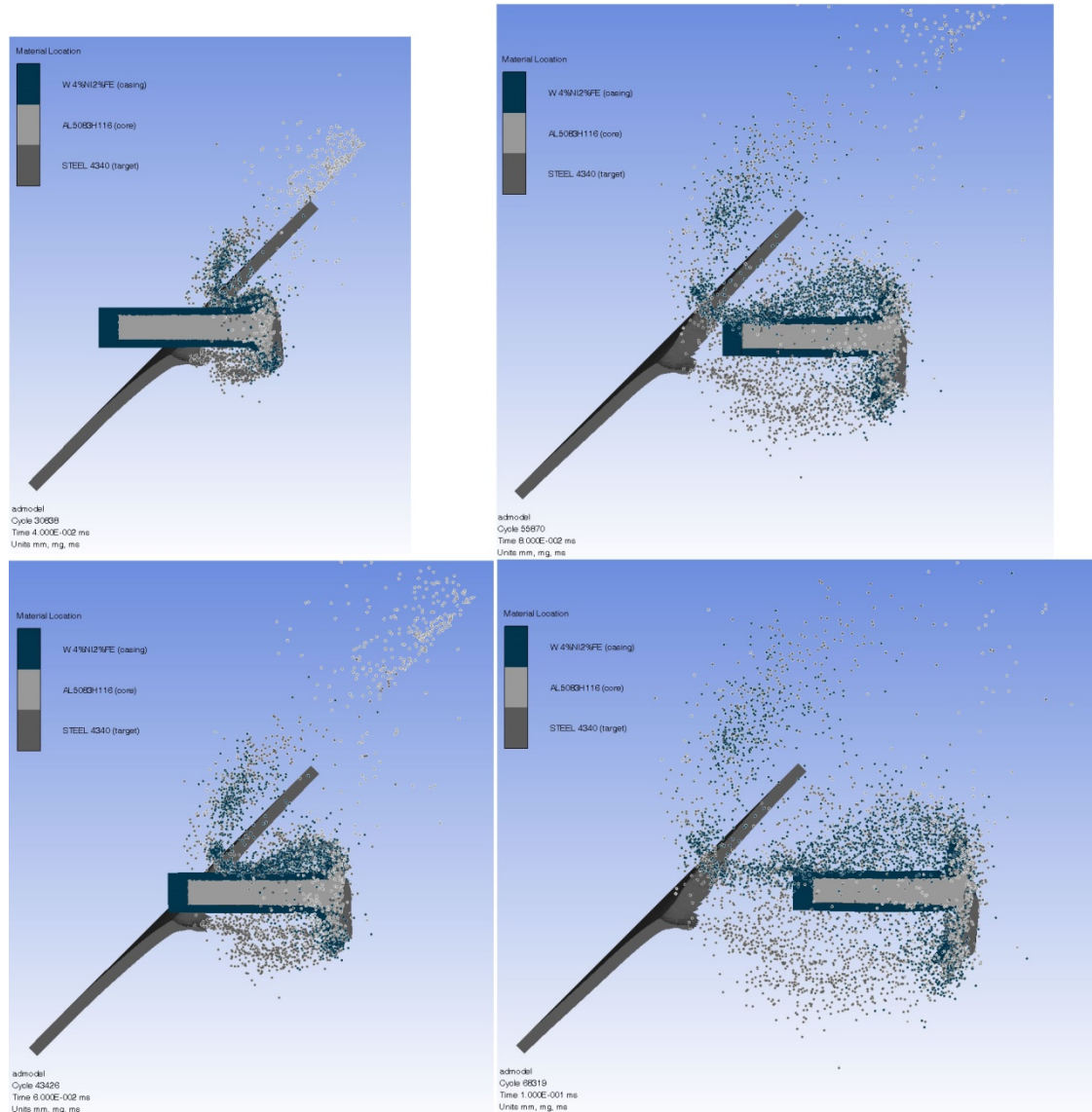


Figure 9. The processes of target penetration and casing fragmentation of PELE into the target with 45° obliquity, for different times (40 μ s, 60 μ s, 80 μ s, and 100 μ s)

Fig. 8 shows the processes of target penetration and casing fragmentation of PELE into the target with 60° obliquity, for different penetration times (40 μ s, 60 μ s, 80 μ s, and 100 μ s). Fig. 8 is interesting because a significant number of fragments are created, although a good part of them ends up in front of the target.

Of them, there are several larger fragments originating from projectile casing that are thrown up in front of the target (Fig. 8) - this phenomenon is not present for smaller target obliquity angles. After 40 μ s, less than half of the projectile has passed through the target (even slower penetration than in the case of 0° and 30° target inclinations).

For this target obliquity, a large spray of fragments from the core, target and casing is created in front of the target and very close to it. There is even greater erosion of the projectile core (compared to other target obliquities), and a very deformed target plug is located on the lower front side of the projectile. After 60 μ s, a larger number of fragments are created around the projectile than in the case when the target has a smaller slope. The radial dispersion of these fragments is similar to that of the 45° tilt target, but a larger number of fragments are present. The deformation of the core and the front part of the casing is significant. After 80 μ s, the deformation of the front part of the casing increases even more.

The radial dispersion of the fragments is greater than at the moment of 60 μ s. This also applies at a time of 100 μ s, where, also, the casing deforms even more at the frontal part and asymmetrically. There is also a greater number of fragments from the core in relation to the smaller tilting angles of the target. Also, the opening in the target is much larger than for smaller target slopes. The spray of fragments is larger on the lower side - an asymmetric beam of fragments is created (for a realistic case of an armored vehicle, this beam would be directed downwards, towards the vehicle floor). Generally, for a target angle of 60°, residual velocity of projectile is in the range of 820.8 m/s (lower part of PELE) to 840.1 m/s (frontal part).

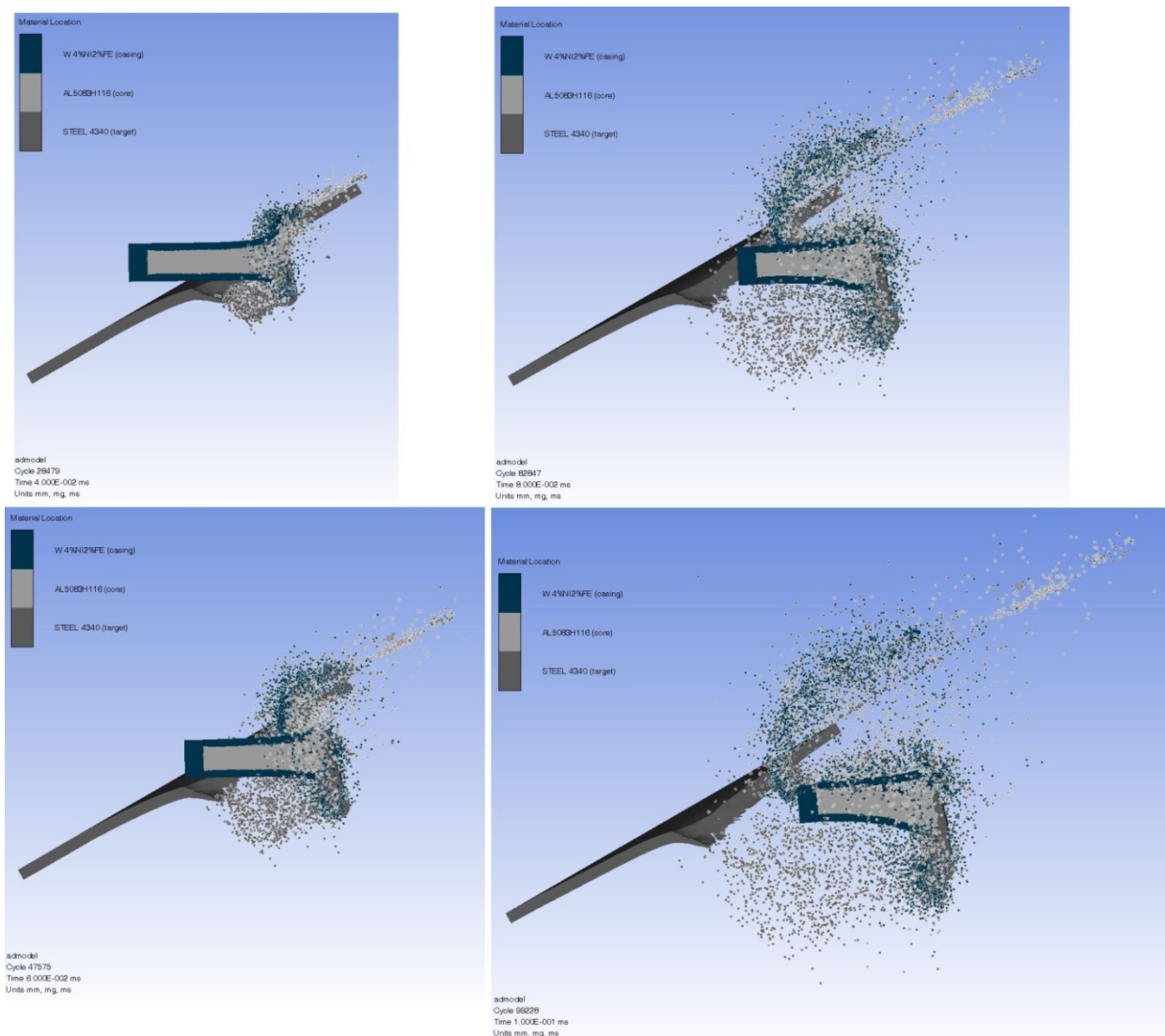


Figure 10. The processes of target penetration and casing fragmentation of PELE into the target with 60° obliquity, for different times (40 μ s, 60 μ s, 80 μ s, and 100 μ s)

Figure 9 shows the expansion and deformation of the PELE system after 100 μ s, for four cases of target tilt. Fragments in Fig. 9 are not shown for a clearer presentation of the components of PELE ammunition. It can be seen how the tilt of the target

contributes to the asymmetric deformation of the projectile casing (jacket), and how, at larger target slopes, a good part of the jacket is fragmented in front of the target itself, especially for a target angle of 60°.

It can also be seen that the opening of the hole in the target is about 2x larger for the angle of inclination of the target of 60° compared to the case with the inclination of the target of 0°, so the plug that was torn from the target is also much larger.

At target inclination angles of 30° and 45°, it can be noticed that there was less deformation of the projectile jacket compared to the target angles of 0° and 60°.

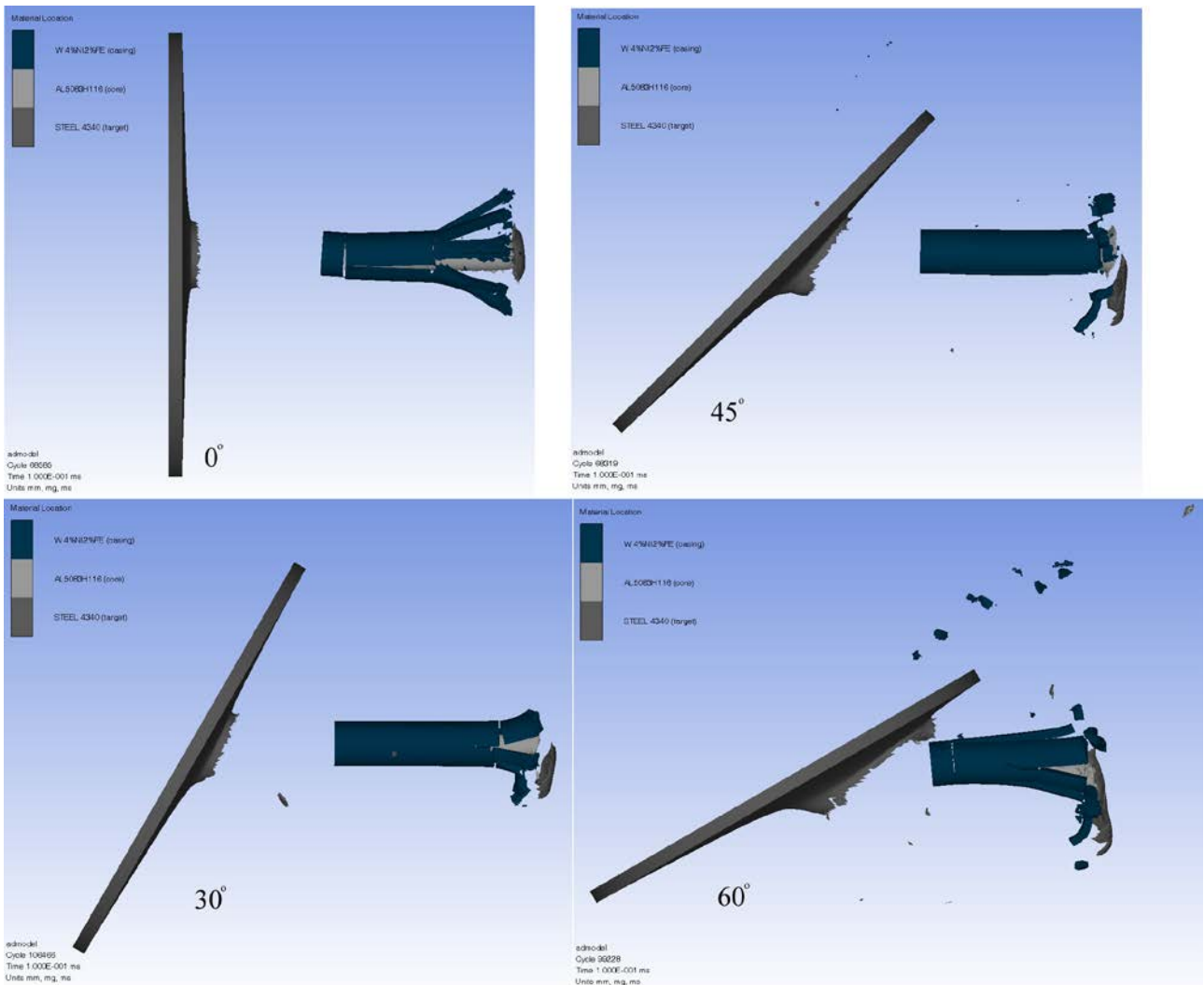


Figure 11. The expansion and deformation of the PELE after 100 μs, for four cases of target tilt

Figure 10 is interesting and shows the fragment velocity vectors after 100 μs (velocity contour values fixed to max 200 m/s since maximal fragment velocity behind target expected is below that value [1]), for four cases of target tilt. Vectors presented correspond with all fragments obtained after the perforation (core, casing, target). It can be seen, firstly, that for a target inclination of 0° the bundle of fragments is almost symmetrical (not entirely due to the stochastic Mott model of fragmentation), and for a target inclination of 60° it is very asymmetric. The velocity vectors (velocity scale is the same/fixed, up to 200 m/s) of the fragments (the length of the velocity vector corresponds to the intensity of the fragment's velocity) show that the highest velocity of the fragments is shown by the case where the target is inclined by 60°, but these fast fragments are mostly lost in front of the target.

The following is the case where the target is at an angle of 0° - there the fast fragments are not lost and act inside the target. The cases of target inclination of 30° and 45° seem to be more favorable from the point of view of protecting the armored vehicle, because the fragment velocities in these cases are much lower compared to targets inclined by 0° and 60°. The velocity vectors of the fragments show that the largest radial dispersion of the fragments, after 100 μs, is present when the target is tilted by 60°. For this case of target inclination, the dispersion is extremely asymmetric, with a good part of the fragments going downwards. It can also be seen that the fragments that originate from the front part of the projectile jacket are faster. Thus, it is shown here that the cases of target tilts of 30° and 45° seem generally more favorable for protection than the other two target tilts.

In order to isolate from these two cases, 35° and 45° inclination of the target, the case that is more favorable from the point of view of protecting the target, the number of larger fragments obtained after the perforation of the target plate was analyzed. It seems that the case of a target inclination of 30° is the most effective in stopping PELE ammunition, for the given type of materials and PELE design, because it shows the lowest number of fragments created but also the lowest velocity of fragments

(previously shown in Fig. 10). After analyzing the fragment number for all target obliquities, it was concluded that the slope of the target of 60° generates by far the largest number of created fragments, but a good part of them ends up in front of the target (Figures 8 and 10). For a 60° inclination of the target, a larger number of more massive fragments are also present. In Fig. 9 they can be seen more clearly.

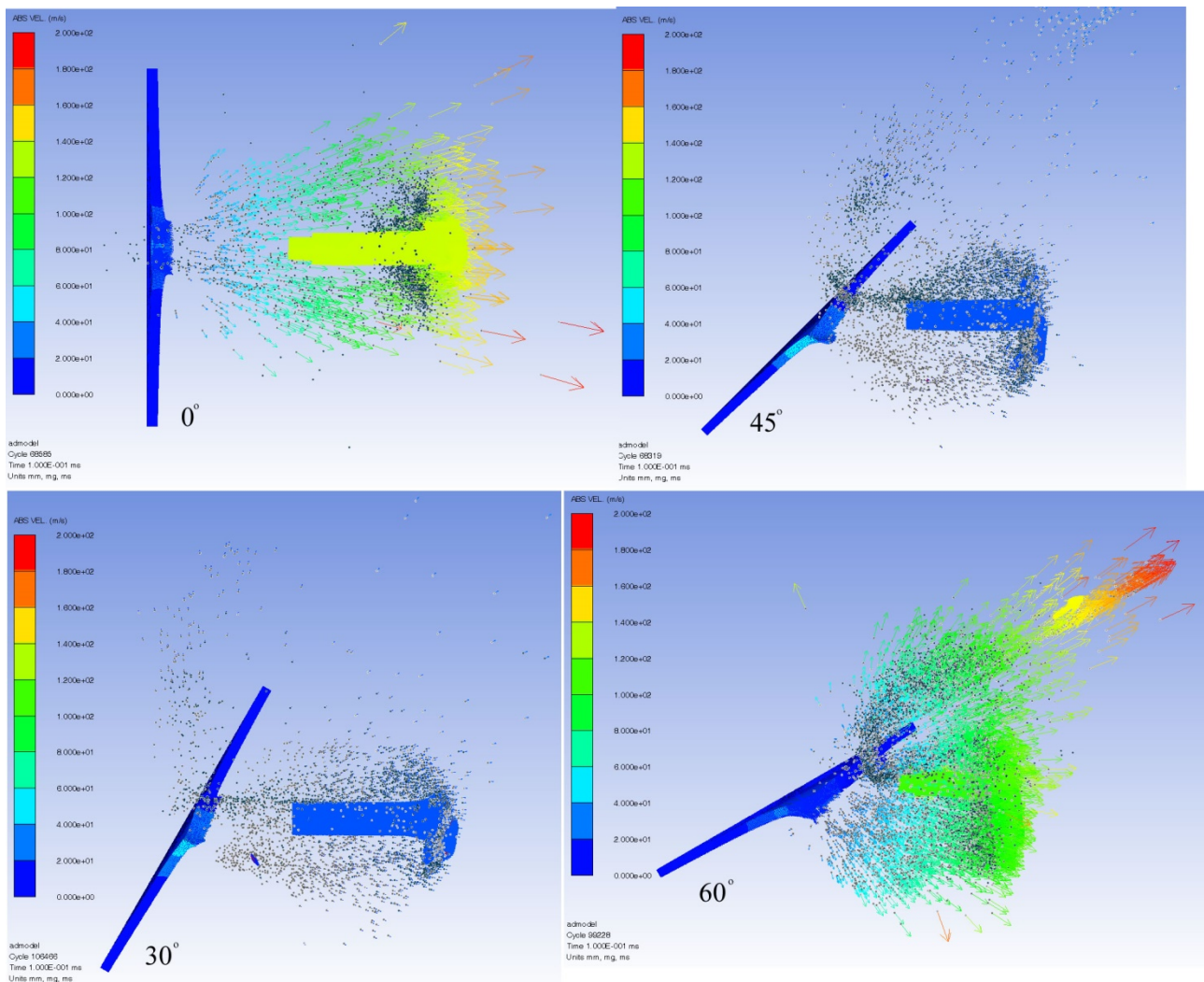


Figure 12. Fragment velocity vectors after 100 μs, for four cases of target tilt

4. Conclusions

In this paper, research on target obliquity influence on efficiency of PELE is analyzed. In that regard numerical simulations were performed with four different target obliquity angles, namely 0°, 30°, 45° and 60°. Before the simulations, the numerical model was successfully validated with available experimental data. The following results in the research were obtained:

- Residual velocity of projectile is smaller for larger target obliquities.

- Plug ejected from the target is visible in front of an aluminum core which was not significantly deformed for 0° target obliquity. The deformation of the aluminum core is more significant for larger target obliquities.
- Target obliquity contributes to the asymmetric deformation of the projectile casing (jacket) and at larger target slopes a good part of the jacket is fragmented in front of the target itself, especially for a target angle of 60°.

- For target obliquities larger than 0° a large spray of fragments from the core goes up, in front of the target, after the impact. An asymmetric bundle of fragments from the target and the jacket is also noticeable for these cases of target inclination, but they are thrown with smaller velocity (in front of the target) because they are more massive.
 - Perforation time for target obliquity angles larger than 0° is longer than when target is at 0°.
 - The lower side of the casing is more deformed than the upper side for target obliquities larger than 0°.
 - The highest velocity of the fragments is shown by the case where the target is inclined by 60°, but these fast fragments are mostly lost in front of the target.
 - Fragments that originate from the front part of the projectile jacket are faster compared to fragments originating from the projectile lower sections.
 - The cases of target inclination of 30° and 45° seem to be more favorable from the point of view of protecting the armored vehicle because the fragment velocities in these cases are much lower compared to targets inclined by 0° and 60°.
 - The opening in the target (perforation hole) is significantly larger for higher target obliquity angles than for smaller ones.
 - For a 60° inclination of the target, a larger number of more massive fragments are present.
 - It seems that the case of a target inclination of 30° is the most effective in stopping PELE ammunition, for the given type of materials and PELE design, because it shows the lowest number of fragments created but also the lowest velocity of fragments.
- [4]. Rittel D., & G. Weisbrod. (2001). Dynamic fracture of tungsten base heavy alloys, *International Journal of Fracture*, 112, 87-98.
- [5]. Reddit forum. (n.d.). *External-preview*. Reddit forum. Retrieved from: https://www.reddit.com/media?url=https%3A%2F%2Fexternal-preview.redd.it%2FWz_jeOYs28emJfV9s_eFEMdLNitn4satzv1GJyZbyM8.jpg%3Fauto%3Dwebp%26s%3D97c850d9994ec9e3f1ef38f44e8300f607446f88&rd=48195. [accessed: 13 March 2024].
- [6]. Rheinmetall Company. (n.d.). *Large calibre – weapons and ammunition*. Rheinmetall Company. Retrieved from: <https://www.rheinmetall.com/en/products/large-calibre/large-calibre-weapons-and-ammunition> [accessed: 14 March 2024].
- [7]. NDIA. (2005). *105/120/125 mm PELE Firing Results*. NDIA. Retrieved from: <https://ndiastorage.blob.core.usgovcloudapi.net/ndia/2005/garm/wednesday/bornngen.pdf> [accessed: 14 March 2024].
- [8]. Zhou J., Ran X., Tang W., Zhang K., Wang H., Chen P., & Ding L. (2023). Research on the penetration characteristics of PELE projectile with reactive inner core, *Polymers*, 15(3), 617.
- [9]. Xu L., Du C., Cheng C., Wang X., Wang J., Du Z., & Gao G. (2021). Effect of projectile parameters on opening behavior of PELE penetrating RC target, *Defence Technology*, 17(3), 859-873.
- [10]. Liu Y., Xu L., Zheng H., Xu M., Lu W., & Du Z.. (2023). Experimental study on the effect of fracture strain on the fragmentation effect of PELE, *Lat. Am. j. solids struct*, 20(7).
- [11]. Ding L., Zhou J., Tang W., Ran X., & Cheng Y. (2018). Damage characteristics of PELE projectile with gradient density inner core material, *Materials*, 11(12), 2389.
- [12]. Cheng C., Xu L., Du Z., Pang Z., Wang M., Sun Y., & Chen X. (2020). Perforation characteristics of metal target plate subjected to PELE, *Lat. Am. j. solids struct*, 17(4).
- [13]. Fan Z., Ran X., Tang W., Ke Y., & Li Z. (2016). The model to calculate the radial velocities of fragments after PELE penetrator perforating a thin plate, *International Journal of Impact Engineering*, 95, 12-16.
- [14]. Jo J., & Lee Y.S. (2012). Numerical simulation of failure mechanism of PELE perforating thin target plates, *Trans. Korean Soc. Mech. Eng. A*, 36(12), 1577-1583.
- [15]. Ding L., Tang W., Ran X., Fan Z., & Chen W. (2019). Theoretical model of the axial residual velocity of PELE projectiles penetrating thin metal targets, *Symmetry*, 11(6), 776.
- [16]. Wu G., Wang X., Ji C., Zhao C., & Zhu H. (2020). Numerical simulation analysis of PELE penetrating target plates with different thicknesses, *Vibroengineering Procedia*, 33, 182-187.
- [17]. Ding L., Zhou J., Ran C., Tang W., Xue X., & Zhao Y. (2020). Theoretical model of radial scattering velocity of fragments of the reactive core PELE projectile, *Symmetry*, 12(7), 1190.

References:

- [1]. Paulus G., & Schirm B. (2006). Impact behavior of PELE projectiles perforating thin target plates. *International Journal of Impact Engineering*, 33, 566-579.
- [2]. Ding, L., Zhou, J., Tang, W., Ran, X., & Cheng, Y. (2018). Research on the crushing process of PELE casing material based on the crack-softening algorithm and stochastic failure algorithm. *Materials*, 11(9), 1561.
- [3]. Rheinmetall Company. (n.d.). *The medium calibre ammunition family of Rheinmetall*. Rheinmetall Company. Retrieved from: <https://www.rheinmetall.com/en/products/medium-calibre/medium-calibre-ammunition> [accessed: 12 March 2024].

- [18]. Ji P., & Wang H. (2011). Ballistic limit and residual velocity of PELE penetrating against metal target, *Journal of Beijing Institute of Technology*, 20(2), 183-186.
- [19]. Ding L. Zhou J., Tang W., & Ran X. (2019). Damage characteristics analysis of the truncated cone-shaped PELE projectile, *Symmetry*, 11(6), 776.
- [20]. Tu, S., Wang, J., An, Z., & Chang, Y. (2009). Influence of thickness of armor on the burst-effect of steel shell PELE. In *2009 9th International Conference on Electronic Measurement & Instruments*, 4-926. IEEE.
- [21]. Yin J.P., Han Y.Y., Wang X.F., Chang B.H., Dong F.D., & Xu Y.J. (2019). A new charge structure based on computer modeling and simulation analysis, *Journal of Visual Communication and Image Representation*, 64.
- [22]. Verreault J. (2015). Analytical and numerical description of the PELE fragmentation upon impact with thin target plates, *International Journal of Impact Engineering*, 76, 196-206.
- [23]. Modelling Fragmentation Events in AUTODYN. (1999). IHG Livingstone, Century Dynamics Ltd., AUTODYN User Group Meetings.
- [24]. Catovic, A. (2023). Research of influence of different shaped charge liner materials on penetration depth using numerical simulations, *Periodicals of Engineering and Natural Sciences*, 11(4), 1-26.
- [25]. Grady D. (1988). The spall strength of condensed matter, *J. Mech. Phys. Solids*, 36, 353-384.
- [26]. Bless S.J., Tarcza K., Chau R., Taleff E., & Persad C. (2006). Dynamic fracture of tungsten heavy alloys, *International Journal of Impact Engineering*, 33, 100-108.
- [27]. Ansys Autodyn Help Viewer. (2016). Version 17.2.0. Retrieved from: <https://innovationspace.ansys.com/innovation-learning/> [accessed: 22 March 2024].
- [28]. Thyssenkrupp. (2017). *Material Data Sheet*. Thyssenkrupp. Retrieved from: https://ucpcdn.thyssenkrupp.com/_legacy/UCPthyssenkruppBAMXUK/assets.files/material-data-sheets/aluminium/5754.pdf [accessed: 18 March 2024].
- [29]. Matweb. (n.d.). *ASM Aerospace Specification Metals Inc.* Matweb Retrieved from: <https://asm.matweb.com/search/SpecificMaterial.asp?bassnum=ma5083h116> [accessed: 18 March 2024].
- [30]. Mubashar A., Uddin E., Anwar S., Arif N., Waheed S., & Chowdhury M. (2019). Ballistic response of 12.7 mm armour piercing projectile against perforated armour developed from structural steel, *Proc IMechE Part L: J Materials: Design and Applications*, 233(10), 1993-2005.
- [31]. Hazell P. (2023). *Armour - Materials, Theory, and Design*, (2nd ed.). CRC Press.
- [32]. Johnson G. R. (1985). Fracture characteristics of three metals subjected to various strains, strain rates, temperatures and pressures, *Engineering Fracture Mechanics*, 21(1), 3148.
- [33]. Johnson G., & W.A. Cook. (1983). A constitutive model and data for metals subjected to large strains, high strain rates and high temperatures. *Proceedings 7th International Symposium on Ballistics*, 541-547.
- [34]. Zukas, J. (1990). *High velocity impact dynamics*. Wiley Interscience.